접착 및 계면 제20권 제4호, 2019년
〈연구논문(Original Article)〉

Journal of Adhesion and Interface Vol.20, No.4, 2019
http://dx.doi.org/10.17702/jai.2019.20.4.155

코페이셜 적층 구조를 가진 펜타센 유도체 단결정기반 유기트랜지스터의 계면 전하이동 이방성에 관한 연구

최현호†

경상대학교 나노신소재공학부

(2019년 12월 05일 접수, 2019년 12월 12일 수정, 2019년 12월 16일 채택)

Interfacial Charge Transport Anisotropy of Organic Field-Effect Transistors Based on Pentacene Derivative Single Crystals with Cofacial Molecular Stack

Hyun Ho Choi†

School of Materials Science and Engineering, Gyeongsang National University, Jinju 52828, Korea

(Received December 05, 2019, Revised December 12, 2019; Accepted December 16, 2019)

요 약 : 공액분자 나노구조체 계면에서의 전하이동 이방성을 이해하는 것은 유기전계효과트랜지스터(OFET)에서 구조-물성 상관관계를 규명하는데 중요하다. 본 연구에서는 대표적인 코페이셜 적층구조를 가진 6,13-bis(triisopropylsilylethynyl) pentacene (TIPS-pentacene) 유기반도체 단결정과 산화물 계면에서 전하이동도 이방성을 연구하였다. 용매치환공정을 이용해 유기단결정을 산화실리콘 절연체 표면에 성장시키고 유기단결정/산화물 계면에서 전하이동을 유도할 수 있도록 OFET 소자를 완성하였다. TIPS-pentacene OFET에서 최고/최저 전하이동도 이방성은 5.2로 관찰되었다. TIPS-pentacene의 전하이동을 담당하는 공액부의 최인접부와의 상호작용을 분석한 결과, HOMO 준위 커플링과 전하의 호핑 궤도가 전하이동도 이방성에 기여하는 것으로 밝혀졌다. HOMO 준위 커플링에 기반한 전하이동도 이방성의 정량적 예측은 실험결과와 유사하게 나타났다.

Abstract: Understanding charge transport anisotropy at the interface of conjugated nanostructures basically gives insight into structure-property relationship in organic field-effect transistors (OFET). Here, the anisotropy of the field-effect mobility at the interface between 6,13-bis(triisopropylsilylethynyl) pentacene (TIPS-pentacene) single crystal with cofacial molecular stacks in a-b basal plane and SiO gate dielectric was investigated. A solvent exchange method has been used in order for TIPS-pentacene single crystals to be grown on the surface of SiO_2 thin film, corresponding to the charge accumulation at the interface in OFET structure. In TIPS-pentacene OFET, the anisotropy ratio between the highest and lowest measured mobility is revealed to be 5.2. By analyzing the interaction of a conjugated unit in TIPS-pentacene with the nearest neighbor units, the mobility anisotropy can be rationalized by differences in HOMO-level coupling and hopping routes of charge carriers. The theoretical estimation of anisotropy based on HOMO-level coupling is also consistent with the experimental result.

Keywords: *organic field-effect transistor, mobility anisotropy, TIPS-pentacene, cofacial stack*

† Corresponding author: Hyun Ho Choi (hh.choi@gnu.ac.kr)

1. Introduction

In organic semiconductors, particularly organic small molecules, it has been a matter of common interest to understand the relationship between charge carrier mobility and molecular stacking of conjugated moieties [1-7]. Acene groups, including anthracene, tetracene, and pentacene, are popular conjugated moieties of organic small molecules, so it is highly valuable to estimate the intermolecular charge transfer with variable intermolecular stacking of acene moieties. The most effective intermolecular charge transfer is when the conjugated moieties are cofacially stacked. For this reason, several groups have theoretically proposed the relationship between electronic band structure and intermolecular charge transfer of acene moieties when they are cofacially stacked[3, 7, 8]. The cofacial stack can be basically described by two parameters: intermolecular distance and lateral displacement[8]. The band width calculation estimated the transfer integral, which follows the exponential decay with the increase of intermolecular distance and the periodical oscillation with lateral displacement[7, 8]. For the experimental verification, several groups have synthesized acene derivatives with relevant crystallography containing cofacial stacks. However, fully cofacial configurations are rarely encountered in crystals because acene molecules prefer to form herringbone structure.

A 6,13-bis(triisopropylsilylethynyl) pentacene (TIPS-pentacene), firstly suggested by Anthony et al.[9] contains pentacene moiety for charge transport. However, in contrast to pentacene, it prefers cofacial stack because the triisopropylsilylethynyl side groups interrupt the herringbone packing of pentacene. Furthermore, on the a-b basal plane, the intermolecular distance and the lateral displacement of pentacene moieties are not isotropic, which is effective to experimentally verify the relevance of the theoretical estimation, that is transfer integral as a function of intermolecular distance and lateral displacement. Here, we explored the mobility anisotropy of charge carriers in TIPS-pentacene single crystal and examined the relationship between molecular stacking and charge mobility. In particular, the charge transport at the surface of TIPS-pentacene single crystal has been analyzed by fabricating organic field-effect transistor (OFET) device.

2. Experiment Section

Devices were fabricated on SiO_2 (300 nm)/Si substrate where SiO2 and Si were used as gate insulator and gate electrode in OFET device, respectively. To terminate hydroxyl groups exposed on SiO_2 surface that is defective to charge transport, the SiO_2 surface was chemically modified with octyltrichlorosilane (OTS) by baking (120 °C, 20 min) followed by dipping in OTS

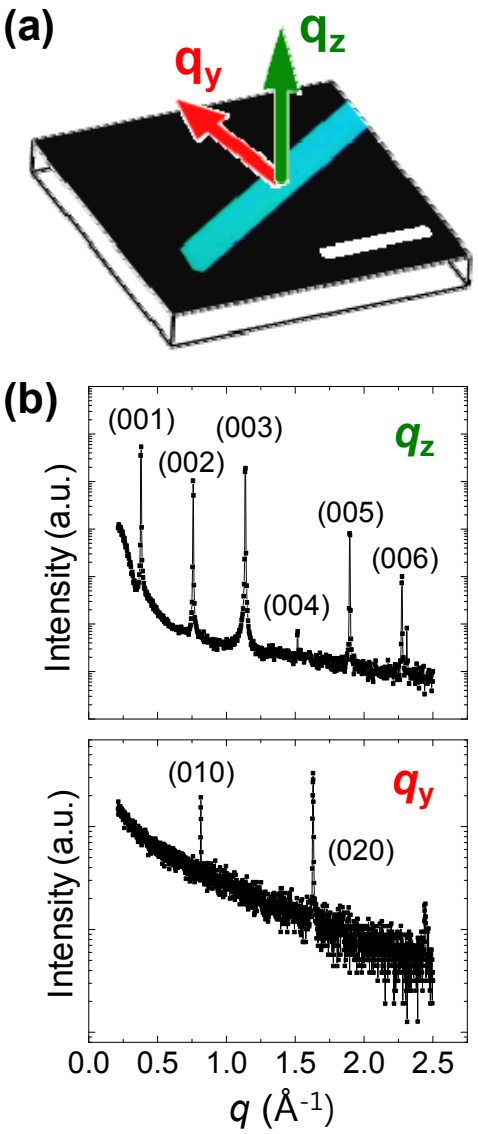

Figure 1. (a) Polarized optical microscopy image of TIPS-pentacene single crystal. (b) X-ray diffraction patterns of the single crystal with stacking direction along q_z (out-of-plane, top) and q_y (in-plane). The scale bar shown on panel a is 100 μm.

solution[10-13]. The TIPS-pentacene single crystals were grown by using solvent exchange method in the solution phase by following the previous literature[14]. A 50 μL of the concentrated toluene solution (10 mM) of TIPS-pentacene was injected into 10 mL acetonitrile. TIPS-pentacene molecules start to self-assemble to make single crystals after the injection. The total growth time was over 4 hours, to allow TIPS-pentacene molecules to be sufficiently self-assembled. The final products were predominantly straight thin plate-like crystals. Well-grown crystals exhibiting a uniform birefringence in the polarized optical microscope were used in further device fabrication. Au electrodes (source and drain) were deposited on the top of TIPS-pentacene crystal through a shadow mask using thermal evaporation. The shadow mask was selectively aligned along the crystal orientations.

The morphology of the organic single crystal was analyzed with a Veeco NanoScope IIIa atomic force microscopy. The molecular ordering was analyzed using X-ray diffraction (theta-2theta mode) at the 10C1 beamline of Pohang Acceleration Laboratory. All OFETs were characterized with a Keithley S4200.

3. Results and Discussion

Fig. 1a shows an optical microscopy image of a TIPS-pentacene single crystal. The crystals grown by our method are typically formed as elongated hexagon or parallelogram thin plates with the following dimensions: thickness of 0.1-1 μm, width of 4-100 μm (short-axis), and length of 100-800 μm (long-axis). The molecular orientation of the single crystal was revealed by X-ray diffraction (XRD) as shown in Fig. 1b. The XRD results revealed that the normal to the crystal surface corresponds to (001), and the short-axis corresponds to (010), consistent with previous TEM results[15, 16]. The XRD data of the single crystal and powder diffraction data confirmed the long-axis corresponding to (100)[9].

As shown in Fig. 2a, the source-drain was patterned along long axis (type L, left panel) and short axis (type S, right panel). The homogeneous birefringence as shown in inset of Fig. 2a that is polarized optical microscopy image represents that TIPS-pentacene single crystals had few intrinsic defects and were well-contacted with the substrate. The channel length was 50 μm and the effective channel width, that is proportional to the crystal size, was measured in the middle of channel gap. Fig. 2b shows the typical transfer characteristic of the type S device at the saturation regime in air. The mobility is 0.13 $cm^2V^{-1}s^{-1}$ and current on/off ratio, on/off current ratio, I_{on}/I_{off} is 10^7. A weak dependence of the mobility on the applied gate voltage indicates that the contact resistance is small compared to the channel resistance[17, 18]

Fig. 3 shows the representative transfer curves of L and S devices. Since the drain current (I_D) is proportional to the channel width, the I_D was normalized by W/L. The field-effect mobility, μ_{FET} was calculated at the saturation regime using the following equation:

$$\mu_{FET} = \frac{2}{C_i}\left|\frac{\partial\sqrt{(L/W)\cdot I_D}}{\partial V_G}\right|^2 \quad \text{Eq. 1}$$

where C_i is the capacitance (11 $nFcm^{-2}$). In accordance with Eq. 1, the mobilities for L and S devices were proportional to the slope of the $[(L/W)I_D]^{1/2}$ as shown in Fig. 3. The mobility maximum was 1.42 $cm^2V^{-1}s^{-1}$, which was observed in L device. The relatively low mobility of our device in comparison with the record value is attributed to 1) the substantial thickness of crystals that is significantly deficient in charge injection as well as charge transport, and 2) the presence of chemical impurities that provide charge traps in the conduction channel of TIPS-pentacene. The photoconductivity measurements done by Ostroverkhova et al. also revealed that the maximum mobility was obtained when the device was aligned along close-to-L direction[19]. In our experiment, more than 10 single crystals of each type were measured. The average values of the mobility for type L and S devices, μ_L and μ_S were 0.85 ± 0.21 $cm^2V^{-1}s^{-1}$ and 0.16 ± 0.08 $cm^2V^{-1}s^{-1}$, respectively. The anisotropy ratio, μ_L/μ_S of the average value and the maximum value of the mobility was 5.3 and 5.2, respectively. Interestingly, it is higher than that of rubrene[20-22], tetracene[23], pentacene[24], and cyclohexyl-substituted quarterthiophene[17], which are categorized into herringbone-stacked materials. Furthermore, even in TIPS-pentacene, this ratio is higher than that extracted from the transient photoconductivity measurement, which is typically used to understand the charge transport in bulk[19].

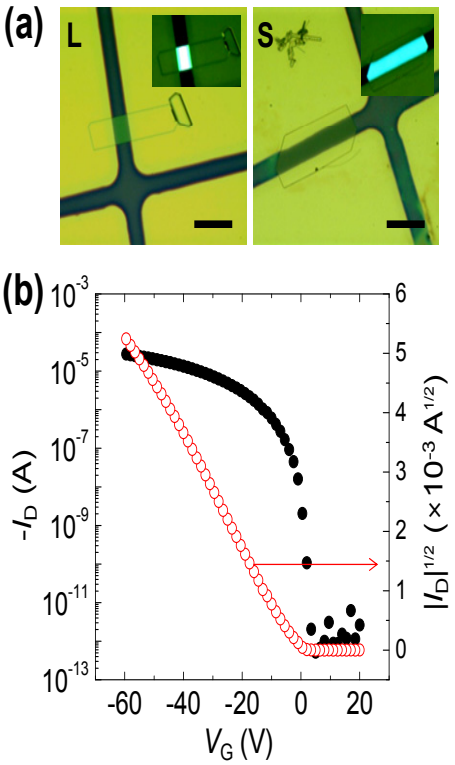

Figure 2. (a) Optical and polarized optical (inset) microscopy images of TIPS-pentacene single crystal OFETs. Source-drain electrode was selectively aligned along long-axis, L (left) and short-axis, S (right) of TIPS-pentacene single crystal. (b) Typical transfer characteristic of TIPS-pentacene single crystal OFET in the saturation regime at a fixed V_{SD} = -60 V. The scale bar shown on panels a and b is 100 μm.

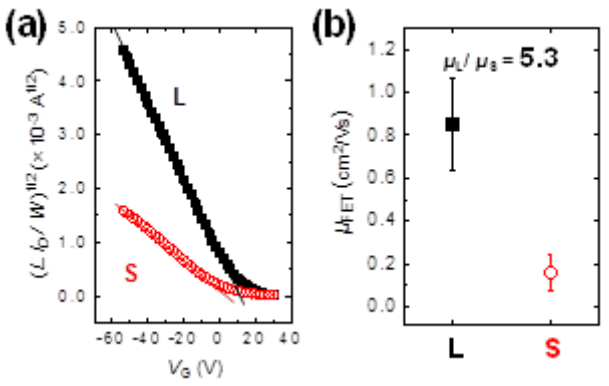

Figure 3. (a) The transfer characteristics of the L and S devices where V_G is the applied gate voltage. (b) Summary of field-effect mobility representing mobility anisotropy.

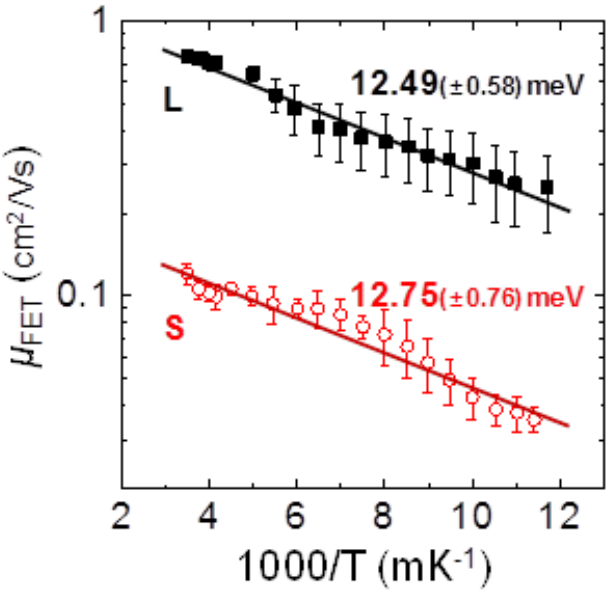

Figure 4. Temperature dependence of the field-effect mobility along L and S directions of the TIPS-pentacene single crystal. The slope of the linear plot is related with the activation energy, E_a.

To understand the origin of mobility anisotropy, we investigated the temperature dependence of the mobility along each direction. Fig. 4 shows temperature-dependent field-effect mobility of L and S devices.

The mobilities were measured from 90 K to 290 K under the vacuum. The mobilities along both directions follow Arrhenius relation[4, 25]: $\mu_{FET}(T) = \mu_0 \cdot \exp[-E_a/(k_B T)]$, where E_a is the average activation energy of charge traps. It could be inferred that the carrier transport in our system follows polaron hopping or multiple-trapping and release model[1-3]. The interesting observation is that the Ea was independent of molecular orientation, in which Ea is 12.49 meV for the L device and 12.75 meV for the S device. Based on the fact that the activation energy isotropy has been also observed in rubrene and tetracene single crystal OFETs[20, 23], this result indicates the density of state of localized energy levels at the interface between TIPS-pentacene single crystal and OTS-treated SiO_2[23]. The activation energy isotropy results in the temperature-independent anisotropy ratio. Therefore, even though the charge carriers follow incoherent trap-assisted transport, the mobility anisotropy is solely attributed to intrinsic difference in physical property such as molecular stacking.

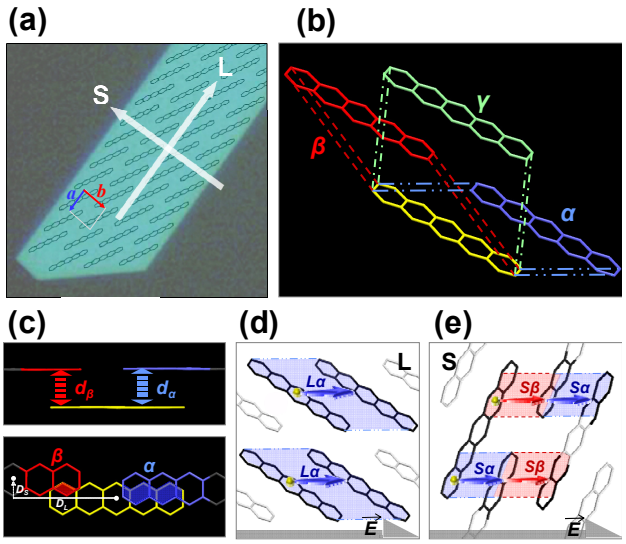

Figure 5. (a) The SEM image of TIPS-pentacene single crystal with schematical stacking of pentacene fragments in the *a-b* basal plane. (Scale bar=20 μm) (b) Three kinds of the nearest neighbor pentacene fragments in TIPS-pentacene single crystal: α, β, and γ. (c) The intermolecular distance (up) and the lateral displacement (down) of α and β stacking (d_α and d_β) . DL and DS are pentacene fragment's long- and short-axis displacement, respectively. The hopping routes of (d) L and (e) S devices along the electric field. α stacking is the main path for L devices (Lα). However, the alternating α and β stacking are the hopping route for S device (Sα and Sβ).

The calculation on band electronic structure has proposed that the mobility anisotropy is larger in cofacially structured materials than that in herringbone structure ones. Haddon et al. calculated the band width along a, b, and c directions of TIPS-pentacene unit cell based on the Extended Huckel theory[26]. The simulation reported that the valence band width was five times wider along a direction than along b direction. Compared to pentacene which has herringbone structure, TIPS-pentacene has a higher value of the anisotropy ratio in band widths. According to the band transport model, the mobility increases with an increase of band width[4]. It means that TIPS-pentacene crystal with cofacial stacks has larger anisotropy ratio than pentacene crystal with herringbone stacking. However, because the hopping mechanism was active in our OFET devices, it is inadequate to explain the anisotropy ratio of the field-effect mobility with band widths. When the hopping transport is active, the mobility is proportional to the hopping rate, which is proportional to the square of the electronic coupling between conjugated molecules according to the Marcus theory[1-3, 5, 6]. Thus, we tried to explain the anisotropy ratio of the field-effect mobility in TIPS-pentacene single crystal by understanding the electronic coupling between TIPS-pentacene molecules.

It has been reported that the mean-free-path of carriers is about 1 lattice constant in organic semiconductors. Based on this, a positive polaron activated on a pentacene unit in TIPS-pentacene hops to the nearest hopping sites along the drain electric field. From the XRD results, the stacking of pentacene fragments in the a-b basal plane of TIPS-pentacene single crystal was schematically drawn onto the SEM image as shown on in Fig. 5a. It was recognized that the pentacene unit of arbitrary TIPS-pentacene molecules at (a, b) has 3 kinds of the nearest neighbors on a-b basal plane: (a+1, b), (a-1, b+1), and (a, b+1). We labeled them α, β, and γ, respectively. Although α, β, and γ stack cofacially, intermolecular distance and lateral displacement along long and short molecular axes are different (Fig. 5b). The intermolecular distance of γ was 6.780 Å, twice longer than that of α (3.401 Å) or β (3.355 Å). Because the mobilities exponentially drop with an increase of intermolecular distance [3, 4, 7, 8], the probability of hopping along γ stack is much lower than that of α or β stacks. Thus, it was concluded that α and β are main routes for the carrier hopping.

As shown in Fig. 5c, the main difference between α and β stacking is the lateral displacement. It causes the difference in electron coupling. It should be noted that when we measured the field-effect mobility, the Fermi level in the channel region shifted toward HOMO of TIPS-pentacene. So, we think that the energy levels of the majority carriers locate near HOMO level and the field-effect mobilities of TIPS-pentacene are more strongly affected by the HOMO-coupling (HMC) than other mobility measurements. Troisi et al. computed the intermolecular HOMO-coupling (HMC) of pentacene couples that stack cofacially as a function of the intermolecular distance and long- and short-displacement [27]. The long-displacement (D_L) and short-displacement (D_S) of α are 6.699 and 0.889 Å, respectively, and those of β are 9.498 and 1.677 Å (Fig. 5c). According to the computation, HOMO-couplings (HMC) of α and β are 237.8 and 34.3 cm-1, respectively.

From the classification of the molecular stacking, we could simply explain the carrier mobility anisotropy in our experiment. When the carrier transports along L-direction, α stacking is the main path for the intermolecular hopping (Lα) as shown in Fig. 5d. On the other hand, when the carrier transports along S-direction, α and β stacks alternate in the transport route (Sα and Sβ). This difference in hopping route is the primary origin of the mobility anisotropy. As discussed above, H-H of α stacking was much higher than that of β stacking, thus the mobility of the S devices in which β stacking is inserted could be lower than that of the L devices.

Because the inserted could be lower than that of the L devices. mobility anisotropy. As discussed above, H-to the direction of drain electric field in L or S device, the angle between π-stacking direction and drain electric field takes into account for calculating hopping rate. The hopping rate could be maximized when the hopping direction and π-stacking direction were parallel but in the case of L and S devices, the intermolecular hopping rate drops from the maximum value. We defined θ, as the angle between the π-stacking direction vector and the drain electric field and assumed that the hopping rate follows the square of cosine function with an increase of θ. Therefore, in the TIPS-pentacene single crystal FET, the hopping rate v_H can be described as

$$v_H \sim (H-H)^2 \cdot \cos^2\theta$$

In the case of L devices, θ_L is 63.3° and 3.3case of L devices, ntacene single crystal FET, the hopping rate the hopping rate follows the sθ_S is 31.0° and the hopping rate can be written as a combination of hopping to route he hopping rateMatthiessenpp rule. In addition, the polaron on a pentacene fragment has one neighbor to hop in the L device (Fig. 5d) but it has two neighbors to hop in the S device (Fig. 5e). Because the mobility is proportional to the hopping rate, the anisotropy ratio of the field-effect mobility can be derived as

$$\mu_L \sim v_{H,L\alpha}, \quad \mu_S \sim \frac{2v_{H,S\alpha}v_{H,S\beta}}{v_{H,S\alpha}+v_{H,S\beta}}, \quad \mu_L/\mu_S = 6.7$$

This higher value of the anisotropy in the calculation than the measured value might be due to the crystal imperfections in the solution-phase self-assembly or the carrier diffusion[4].

4. Conclusion

In summary, we measured the anisotropy of the field-effect mobility in TIPS-pentacene single crystal. The measured mobility anisotropy is larger than those of herringbone stack molecules. The applied gate voltage enhanced the mobility's dependence on HOMO-level coupling, and thus we calculated the anisotropy ratio based on the HOMO-level coupling and distortion of pentacene units. The difference in hopping paths is considered as the main origin of the high anisotropic ratio. Further study is needed to study the anisotropy of the field-effect mobility with another cofacially stacked molecules.

Acknowledgements

This work was supported by the fund of National University Promotion Project, Gyeongsang National University, 2019.

References

1. H. Lee, S. M. Dellatore, W. M. Miller, P. B. Messersmith, *Science*, **318**, 426 (2007).
2. H. Lee, N. F. Scherer, P. B. Messersmith, *Proc. Natl. Acad. Sci.*, 103, 12999 (2006).
3. T. S. Sileika, D. G. Barrett, R. Zhang, K. H. A. Lau, P. B. Messersmith, Angew. *Chemie - Int. Ed.*, **52**, 10766 (2013).
4. X. Zhang, Y. Lv, H. C. Yang, Y. Du, Z. K. Xu, *ACS Appl. Mater. Interfaces*, **8**, 32512 (2016).
5. X. Zhang, P. F. Ren, H. C. Yang, L. S. Wan, Z. K. Xu, *Appl. Surf. Sci.*, **360**, 291 (2016).
6. K. Liu, H. Li, Y. Wang, X. Gou, Y. Duan, *Colloids Surfaces A Physicochem. Eng. Asp.*, **477**, 35 (2015).
7. X. Zhang, M. Liu, X. Zhang, F. Deng, C. Zhou, J. Hui, W. Liu, Y. Wei, *Toxicol. Res.*, **4**, 160 (2015).
8. D. Payra, M. Naito, Y. Fujii, Y. Nagao, *Chem. Commun.*, **52**, 312 (2016).
9. S. Huang, Y. Zhang, J. Shi, W. Huang, *ACS Sustain. Chem. Eng.*, **4**, 676 (2016).
10. H. Ejima, J. J. Richardson, K. Liang, J. P. Best, M. P. Van Koeverden, G. K. Such, J. Cui, F. Caruso, *Science,* **341**, 154 (2013).

11. J. Guo, Y. Ping, H. Ejima, K. Alt, M. Meissner, J. J. Richardson, Y. Yan, K. Peter, D. Von Elverfeldt, C. E. Hagemeyer, F. Caruso, *Angew. Chemie - Int. Ed.*, **53**, 5546 (2014).
12. J. H. Park, K. Kim, J. Lee, J. Y. Choi, D. Hong, S. H. Yang, F. Caruso, Y. Lee, I. S. Choi, *Angew. Chemie - Int. Ed.*, **53**, 12420 (2014).
13. T. G. Shutava, M. D. Prouty, V. E. Agabekov, Y. M. Lvov, *Chem. Lett.*, **35**, 1144 (2006).
14. I. Erel-Unal, S. A. Sukhishvili, *Macromole-cules*, **41**, 3962 (2008).
15. V. Kozlovskaya, E. Kharlampieva, I. Drachuk, D. Cheng, V. V. Tsukruk, *Soft Matter*, **6**, 3596 (2010).
16. B.-S. Kim, H. Lee, Y. Min, Z. Poon, P. T. Hammond, *Chem. Commun.*, **28**, 4194 (2009).
17. M. V. Lomova, A. I. Brichkina, M. V. Kiryukhin, E. N. Vasina, A. M. Pavlov, D. A. Gorin, G. B. Sukhorukov, M. N. Antipina, *ACS Applied .Mater. Inter.*, **7**, 11732 (2015).
18. E. Kilic, M. V. Novoselova, S. H. Lim, N. A. Pyataev, S. I. Pinyaev, O. A. Kulikov, O. A. Sindeeva, O. A. Mayorova, R. Murney, M. N. Antipina, B. Haigh, G. B. Sukhorukov, M. V. Kiryukhin, *Sci. report*, **7**, 4159 (2017).
19. A. Shukla, J. C. Fang, S. Puranam, F. R. Jensen, P. T. Hammond, *Adv. Mater.*, **24**, 492 (2012).
20. X. F. Huang, J. W. Jia, Z. K. Wang, Q. L. Hu, *Chinese J. Polym. Sci.*, **33**, 284 (2015).
21. M. Shin, J. H. Ryu, J. P. Park, K. Kim, J. W. Yang, H. Lee, *Adv. Funct. Mater.*, **25**, 1270 (2015).
22. K. Kim, M. Shin, M. Y. Koh, J. H. Ryu, M. S. Lee, S. Hong, H. Lee, *Adv. Funct. Mater.*, **25**, 2402 (2015).
23. M. Shin, K. Kim, W. Shim, J. W. Yang, H. Lee, *ACS Biomater. Sci. Eng.*, **2**, 687 (2016).
24. M. Dierendonck, K. Fierens, R. De Rycke, L. Lybaert, S. Maji, Z. Zhang, Q. Zhang, R. Hoogenboom, B. N. Lambrecht, J. Grooten, J. P. Remon, S. D. Koker, B. G. D. Geest, *Adv. Funct. Mater.*, **24**, 4634 (2014).
25. M. Shin, H. A. Lee, M. Lee, Y. Shin, J. J. Song, S. W. Kang, D. H. Nam, E. J. Jeon, M. Cho, M. Do, S. Park, M. S. Lee, J. Jang, S. Cho, K. Kim, H. Lee, *Nat. Biomed. Eng.*, **2**, 304 (2018).